Photogrammetrie • Fernerkundung • Geoinformation 1/2007, S. 35–44, 7 figs., 3 tabs.

3D Treetop Positioning by Multiple Image Matching of Aerial Images in a 3D Search Volume Bounded by LIDAR Surface Models

Ilkka Korpela, Helsinki

Keywords: Forest inventory, remote sensing, single tree, mapping, height estimation, allometric modeling

Zusammenfassung: *Eine Methode zur semi-automatischen räumlichen Positionsbestimmung von Baumkronen*. Die Anwendung besteht in der Erstellung von Baumkarten inklusive Höhenangaben, welche für forstwirtschaftliche Planungsaufgaben von besonderem Interesse sind. Das Verfahren integriert hoch auflösende Bilddaten mit Lidar-Daten gerin-gerer Auflösung. Letztere begrenzen den Suchbereich für die Herstellung des Kronenschlusses in den Bilddaten und dienen als Grundlage für eine sichere Bestimmung der Kronenhöhe.

Abstract: This paper presents a method for semi-automatic 3D positioning of tree tops that can be used for obtaining tree maps of the photo-visible trees and tree heights. Such spatio-temporal, detailed information is usable for many applications in e. g. forestry and landscape management. The method incorporates the use of passive, high-resolution optical images with co-existent low-resolution airborne lidar data. The latter is used for confining the search space of image matching to agree with the volume of photo-visible trees in the upper canopy and for obtaining an accurate elevation model, which is paramount for reliable tree height estimation. The method is presented here and tested with restricted image and field material.

1 Introduction

Remote sensing is applied currently in almost all forest data acquisition. Orthoimages and stereopairs of aerial photographs are used for stratifying the forest into stands, satellite images are employed in the assessment of large areas and airborne laser scanning is used for the mapping of topography and canopies. Advances in the sensor technologies and analysis methods continuously widen the potential scenarios of new forest inventory methods that put to use remote sensing (Leckie 1990, Baltsavias 1999, Petrie 2003, Naesset et al. 2004). Single-tree remote sensing (STRS) that is based on the idea of substituting the field measurements and mapping of individual trees with cost-efficient airborne observations is an example of a field made possible by the development. Digital and automatic, image- and/or lidar-based STRS is a topical domain (See references in Culvenor 2003, Korpela 2004, Pouliot et al. 2005), although the concept of STRS is not entirely novel (Worley & Landis 1954, Talts 1977).

STRS aims at a detailed description of the growing stock that is crucial in most applications of forest inventory. Ideally, it provides the size-distribution of the standing trees per species with the two- or three-dimensional map of trees. Korpela & Tokola (2006) examined the potential of image-based, 2D and 3D STRS. The DBH (stem diameter at 1.3 m height) and volume of individual trees cannot be estimated as accu-

1432-8364/07/2007/0035 $ 2.50

rately with STRS as is it possible in the field. The main reason is the indirect estimation phase with allometric models that results in both random and systematic, tree and stand level errors. The model inaccuracies are coupled with photogrammetric measurement errors in species, tree height and/or crown width. Random errors cancel out effectively, but the aggregate results of STRS at the stand level are liable to systematic offsets. Inclusion of tree heights, i. e. the use of 3D STRS was found to improve the estimation accuracy of both DBH and stem volume considerably in comparison to 2D STRS, in which trees are measured for species and crown dimensions only. In addition, in STRS the growing stock is inherently underestimated since some trees always remain unseen – at least by optical sensors.

In STRS, field calibration is needed for avoiding the systematic errors of the allometric equations. Thus, some field visits seem inevitable if very accurate data is wanted. Because of the inferior accuracy in comparison to field measurements, an applicable STRS system has to provide the measurements and estimates with much lower costs, which calls for automatic procedures. A complete 3D STRS system solves all of the following tasks: (a) tree or crown positioning in 3D, measurements of (b) crown dimensions and (c) tree height, (d) species recognition and (e) allometric estimation of stem size (Fig. 1).

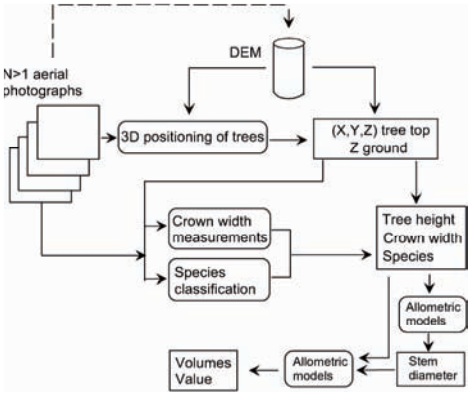

Fig. 1: An example of the data, tasks and output of a 3D image-based STRS-system for stand cruising.

1.1 *Hypotheses and objectives*

This paper addresses the question of using remote sensing for 3D treetop positioning and height estimation and extends the work by KORPELA (2000, 2004), in which a semi-automatic method for treetop positioning was introduced. It was based on the use of multiple image-matching of digitized aerial photographs for the purpose of finding treetops inside a predefined 3D search space in the canopy volume (Fig. 2). The algorithm applies template matching for processing the aerial images into correlation images, where local maxima correspond to 2D image positions of treetops (cf. POLLOCK 1996, LARSEN & RUDEMO 1998). The predefined 3D search space is processed into a point mesh. The points in the mesh are back-projected into the correlation images and aggregated for volumetric correlation, which is further processed into 3D maxima that correspond to candidate treetop positions. The algorithm resembles that of TARP-JOHANSEN (2001), who positioned tree bases of oaks in 3D using multiple leaf-off aerial images. Here, it is further assumed that correct 3D treetop positions will help in solving the other image-based tasks of the measurement of the crown dimensions and the interpretation of species (cf. Fig. 1).

The discernibility of treetops is a major restriction of optical STRS. Only the dominant, co-dominant and intermediate trees are visible with a high likelihood. The probability of discernibility is an exponential function of the relative height of the tree; such probability-of-discernibility curves vary between stands according to the density of the stand (KORPELA 2004). In most cases trees with a relative height of below 50 % are not seen at all in the images. The 50 % relative height constitutes thus a lower limit for the volume from where to conduct the manual or automatic search of treetops – at least in closed canopies. Respectively, the upper limit is at the maximal height of trees. These two parameters vary spatially

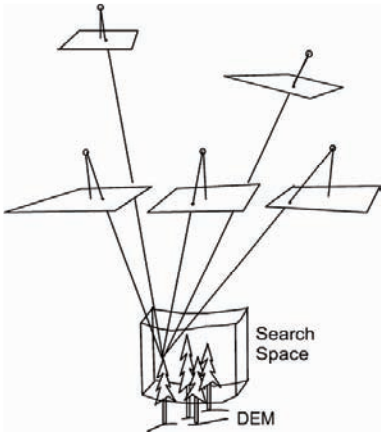

Fig. 2: Image matching for 3D tree top positioning (KORPELA 2004). The search is restricted to a predefined volume in the canopy. A DEM/DTM is used for height estimation. The scale of the images (N > 1) is not restricted as such, but the full orientation of the images has to be established reliably.

and it is necessary to obtain reasonably accurate estimates of them to avoid commission errors by the treetop positioning algorithm (KORPELA 2000, 2004) as the locally restricted depth of the 3D search space is the geometric (epipolar) constraint that is used for the solution of the mathematically ill-posed correspondence problem for tree tops. The results can only be optimal if the search is set to cover the upper canopy volume (KORPELA 2004; p. 35, 65–66).

The estimation of tree height is straightforward once the treetop is positioned in 3D. A DTM gives the elevation of the butt. The error of the height estimate consists thus from possible treetop positioning errors and DTM errors. A DTM is also needed for defining the lower limit of search space at the app. 50 % relative height level below which treetops cannot be expected to be measurable. KORPELA (2004) suggested that an accurate DTM obtained by means of low-resolution laser scanning could be incorporated in the algorithm for the delineation of the search space and for accurate tree height estimation. Similarly, laser scanning was proposed for the estimation of the local, maximal height of trees by a canopy height model (CHM). These proposals/theses are put to test here with real field, image and lidar data. By combining aerial photographs with lidar this paper exploits the principle of the photo-lidar approach presented by ST-ONGE et al. (2004). A low sampling rate airborne lidar is used to keep the material costs to a minimum. The proposal in this article is that low-resolution lidar can be combined with multiple image-matching of aerial images for accurate and cost-efficient, semi-automatic tree top positioning and tree height estimation.

2 Method for semi-automatic 3D treetop positioning using aerial images and LIDAR based surface models

The method consists of the steps 1-9 given below. Automation of steps 2 and computations in step 5 have been developed most in comparison to the algorithm presented in KORPELA 2004.

1) Delineation of the area of interest. Here, the tree tops were positioned inside circular plots with a radius ranging from 15 to 20 m. In general, the geometry of the area of interest can vary and a homogenous stand would be a natural choice in practice.

2) Delineation of the 3D search space in the upper canopy. This is done by analyzing the lidar-DTM and the lidar-CHM such that the search space is filled by a 3D point mesh with 0.5 m spacing. The maximal elevation or local dominant height in a given XY point is given by the CHM, which is multiplied by parameter $f_{HDOM} \in [1, 1.3]$ to reduce the inherent underestimation. Parameter $HDepth \in [0, 1]$ defines the depth of the search space with respect to the local dominant height of trees ($HDepth = 1$) and the terrain elevation ($HDepth = 0$).

3) Selection of a sample tree and the measurement of its 3D treetop position using manual image-matching. The capture of elliptic templates representing the tree in all images (Fig. 3).

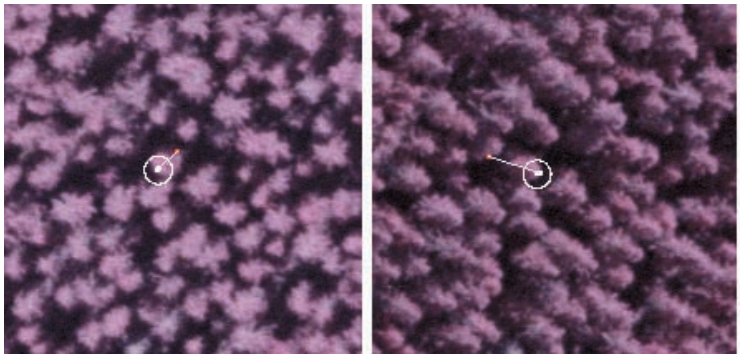

Fig. 3: Template-boundaries of a selected and manually positioned sample spruce tree with parameters: *EllipseHeight* = 3 m, *EllipseWidth* = 2.6 m and *EllipseShift* = -1 m. The shift downwards by *EllipseShift* is seen in the image on the right: the image position of the hot-spot i. e. the tree top and the template centre deviate. The vertical lines connect the measured 3D tree top position and the DTM. This photo-lidar height estimate was 15.53 m and the field measurement was 15.7 m.

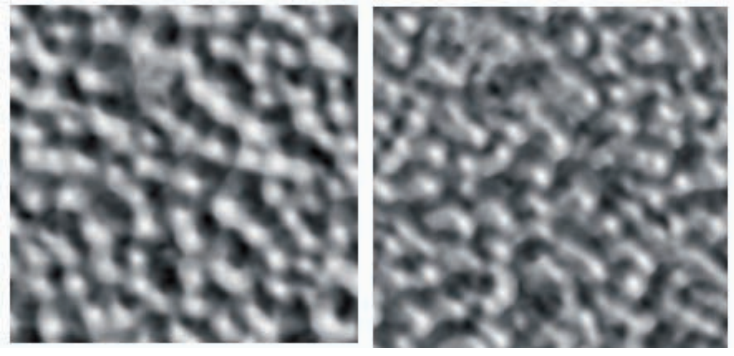

Fig. 4: Cross-correlation images computed using the captured templates and aerial images of Fig. 4. High correlation is displayed in white.

Object space parameters *EllipseShift*, *EllipseHeight*, and *EllipseWidth* define the position, size, and shape of the ellipse in the images. *EllipseShift* shifts the center of the template in the Z direction. Using this parameter, the templates are typically moved down to capture more of the crown than the background. *Ellipseheight* defines the major axis of the elliptic template, which in the images is made parallel to the direction of the Z axis (trunks). *EllipseWidth* defines the length of the shorter axis. The shape is conditioned to circular i. e. the templates are allowed to be elliptic for oblique views only and in the direction of the radial displacement (i. e. Z axis, tree trunk). These 3 parameters take metric values. The actual template images are rectangular copies of the aerial images. Pixels that fall outside the ellipse are masked out. The location of the treetop inside the template, the so called hotspot, is stored for each template and is accounted for in cross-correlation computations that follow.

4) Template matching. Template matching with normalized cross-correlation is carried out for each image using the template of that aerial image. This procedure maps the aerial images into cross-correlation images $\rho(x, y) \in [-1, 1]$, in which high values of ρ indicate good match at image location x, y (Fig. 4).

Ideally $\rho(x, y)$ would consist of very sharp peaks at the correct positions of the treetops.

5) Aggregation of 3D correlation, *ρ3D*. Each point in the search space is back-projected to the cross-correlation images using collinear equations and an affine fiducial mark transformation with pixel accuracy. *ρ3D* is computed for each point in the 3D search space seen as a geometric mean of the images resulting in $\rho 3D \in [0, 2]$.

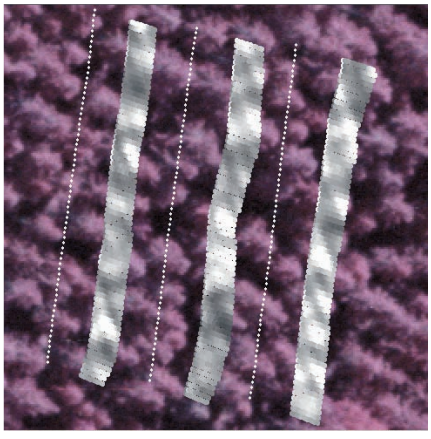

Fig. 5: Illustration of the volumetric, discrete *ρ3D* data in the search space with three transects (slices) superimposed in an oblique aerial view. The brightness of the points denotes *ρ3D*. The undulation is due to changes in terrain elevation and local dominant height of trees. The white dots that form lines are the terrain points.

6) Clustering of the *ρ3D* data into 3D treetop candidate positions. The point set is first sorted in the ascending order of *ρ3D*. Clusters are formed from points with *ρ3D* above a limit, *Rlimit*. Points are merged into existing clusters while the sorted list is processed. Merging is controlled by a planimetric distance parameter, *XYthin*. Points closer than the set value are merged into existing clusters and do not form a new cluster. The 3D position of the cluster is the mean of the 3D points that belong to the cluster and *ρ3D* is used in linear weighting of the coordinates. *Rlimit* is a parameter that controls the quality of the clusters. Only the best clusters are accepted as tree top candidates, if *Rlimit* is set to a high value. In such cases, omission errors are few assuming that the search space is set correctly. A low value of *Rlimit* brings about new clusters at the cost of commission errors. The merge-parameter *XYthin* controls the density of the clusters. A value that is too large causes neighbouring trees to be merged. Similarly, if *XYthin* is set too low it can result in several clusters originating from the actual *ρ3D* response of a single tree.

The description of the steps 7-9 below applies to any practical implementation of the algorithm in situations where no ground truth exists. In the experiments of this study step 7 was replaced by a numerical quality assessment, and steps 8 and 9 were not performed.

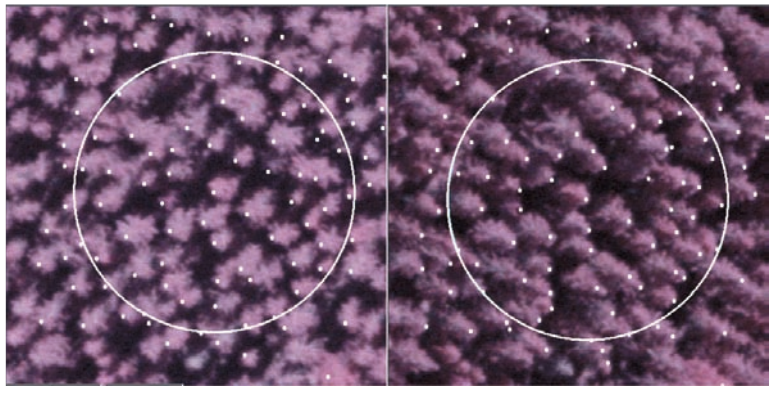

Fig. 6: Candidate positions and the borders of circular photo-plot (r = 15 m) superimposed in an image pair. The circle is drawn at the elevation of the treetop of the model tree.

7) Visual quality assessment of the treetop positioning. The visual evaluation of the matching results is based on visual examination of the candidates that are superimposed either on monoscopic or stereoscopic views. If necessary, the clustering algorithm is re-run by adjusting the parameters *XYthin* and *Rlimit*. Sometimes the procedures have to be repeated from the start by selecting and positioning a new model tree. As all subsequent steps need to be re-computed it is important to have good approximate values for the parameters to avoid unnecessary iteration.

8) Manual correction of the semi-automatic matching results. In it, the bad candidates are removed or corrected for position. The unrecognized tree tops are completed manually using stereo interpretation (for operators with a good stereo vision) or using manual image matching with monocular observations and epipolar constraining (Korpela 2004).

9) Height estimation using the existing DTM.

3 Experiments

3.1 *Data*

The field data in Hyytiälä, southern Finland (61°50′N, 24°20′E) consists of fully mapped and measured stands (Korpela 2004). The field measurement errors for tree positions and the basic tree variables are known through repeated observations. The positions of the field trees have been established with tacheometer and VRS^{TM}-GPS observations and field levelling. The image data consisted of digitized aerial photographs, which have been orientated in one large multi temporal (1946–2004) image block (Korpela 2006). Here, leaf-on images from summers of 2002 and 2004 were used in the experiments. These were taken using standard metric cameras with 15 cm and 21 cm lenses and the images have a 14- or 15-micron pixel size. The experiment allowed for testing the following nominal scales: 1:6000, 1:8000, 1:12000, 1:14000, 1:16000 and 1:30000. The images have forward and side overlaps that vary from 60 % to 80 %. Lidar data was from August 2004 with an Optech ALTM2033 sensor from a flying height of 900 m. The pulses had a footprint diameter of 0.3 m and the pulse density was 1.1 m by 1.3 m, on average. The instrument recorded 1 or 2 returns. The full geometry of each pulse was available: time stamp, position and orientation of the lidar, ranges, intensities and positions of the 1 or 2 returns. A raster DTM was processed from the lidar returns using a simple gradient-based method and a RMSE of 0.30 m was obtained in a test set of 10947 tacheometer points representing terrain of wooded areas. A raster CHM was constructed from lidar maxima in 5 m by 5 m cells.

3.2 *Performance of tree top positioning*

A treetop was considered to be correctly found (hit) if a candidate was inside a 2.4-meter wide and a 6-meter high test-cylinder. The dimensions of the test-cylinder affect the performance measures. The field errors in tree positioning using tacheometer, in height measurements, errors made in updating heights to the time of the photography, possible tree slant and sway as well as the stand density of the test sites were considered. The test-cylinders can have overlap in dense forests and excessive candidates in a test-cylinder or in intersecting cylinders were considered as commission errors and trees without a candidate were considered as errors of omission. A buffer around circular test plots (Fig. 7) was used as trees can be hit by a candidate from the buffer and vice versa.

Hit-rate was the ratio between the number of hits and the total number of trees. An accuracy index was computed based on the numbers of omission (o) and commission (c) errors and the number of trees (n) (cf. Pouliot et al. 2005): $\mathrm{AI} = [(n - o - c)/n] \times 100$. The 3D-positioning accuracy was evaluated with the RMSE that were computed separately for the XY and Z although the positioning is entirely 3D. The RMSEs

include the imprecision of the ground truth and therefore overestimate the true inaccuracy. The positioning error-vector [ΔX, ΔY, ΔZ] was defined as field-candidate; thus a positive ΔZ indicates underestimation. Mean differences of ΔX, ΔY and ΔZ measure systematic offsets. To evaluate the averaging effect of tree heights, a regression line was fitted in the ΔZ × tree height distribution and the slope coefficient (trend) and its standard error were computed. The set of field trees was confined to those that were discernible to the operator. This tree set represents the potential trees to be found. In some stands such a criterion can leave out 50 % or more of the trees; however, the proportion of the total volume in the non-discernible trees is normally small, from 0 % in managed stands to 12 % in natural forests (Korpela 2004).

3.3 *Tests in a spruce stand*

Treetop positioning was tried out using image sets in scales 1:8000–1:16000 (Tab. 1) in one managed spruce stand. Images in the scale of 1:6000 were left out because of the computational burden of template matching and scale 1:30000 was omitted because individual treetops were not well measurable in that scale anymore.

One model tree was used in all trials, and the parameters defining the shape and position of the elliptic templates were kept fixed. The exact 3D position of the treetop was measured separately for each set of images using manual, monoscopic multi-image matching. It varied in Z because of the temporal mismatch of the May 2002 and June 2004 images and because of small orienta-

Tab. 1: Results of treetop positioning using different number of images in different scales. Plot S6 with 95 photo-visible trees in a circular plot with radius of 20 m. $f_{HDOM} = 1.15$, $HDepth = 0.65$.

Number of images, scale, overlaps (%), focal length (cm)	AI-%	c	Mean ΔZ m	RMS ΔZ, m	RMS ΔXY, m
2 1:8000 60/60 21	61.1	13	−0.04	1.29	0.70
2 1:8000 60/60 21	77.9	9	−0.39	1.24	0.73
4 1:8000 60/60 21	85.3	7	+0.06	0.76	0.68
4 1:8000 60/60 21	88.4	5	−0.21	0.99	0.67
6 1:8000 60/60 21	85.3	2	−0.08	0.72	0.61
2 1:12000 70/60 15	82.1	10	+0.22	0.80	0.60
3 1:12000 70/60 15	91.6	5	+0.13	0.70	0.56
4 1:12000 70/60 15	88.4	4	+0.31	0.85	0.57
3 1:14000 80/60 21	87.4	4	−0.09	0.83	0.68
4 1:14000 80/60 21	87.4	7	−0.20	0.93	0.65
6 1:14000 80/60 21	94.7	3	−0.15	0.87	0.60
7 1:14000 80/60 21	93.7	2	−0.12	0.94	0.62
2 1:16000 60/60 15	85.3	5	−0.25	0.87	0.66
3 1:16000 60/60 15	88.4	3	+0.15	0.93	0.62
4 1:16000 60/60 15	74.7	4	+0.42	0.98	0.58

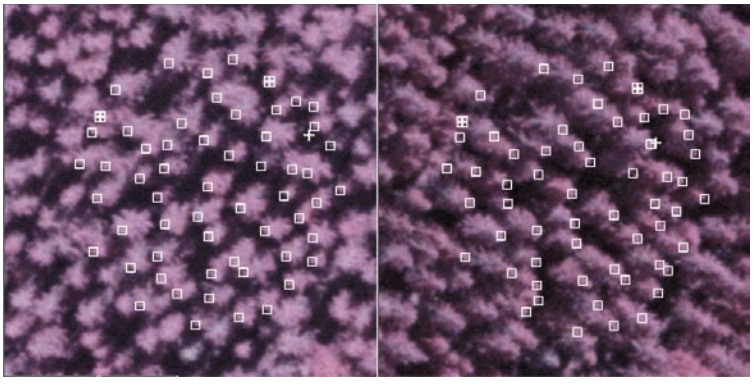

Fig. 7: Results of treetop positioning for a circular test plot. Unfilled squares depict the candidate positions for correct hits (56), squares with a cross depict missed treetop positions ($o = 2$), and the crosses depict the commission errors ($c = 1$). The AI was [(58-2-1)/58] × 100 = 94.8 %. The hit-rate in total stem volume was 97.1 %, RMSE of ΔXY was 0.55 m, RMSE of ΔZ was 0.67 m with a slope coefficient of 0.055 m per m of tree height. The errors in the DTM elevations had an RMS of 0.27 m.

tion and observation errors. The search space was kept fixed with parameters f_{HDOM} and *HDepth*. Tree heights from May 2002 were simply added 0.7 m, which corresponded to the average height growth of three summers. Parameters *Rlimit* and *XYthin* were tuned for obtaining optimal results in the AI-measure.

Increasing the number of images usually improved the performance in the AI measure; however there were images in which the crown of the model tree was not seen against a clear background, which resulted in a poor cross-correlation image that deteriorated treetop positioning. The imaging geometry affects treetop positioning; best results were obtained with an image set that consisted of six images taken with normal-angle cameras at the scale of 1:14000. These images had even large overlaps and the elevation of the sun was higher (45°) during the photography. These factors affect occlusion and shading in aerial views that can impede image matching. It seems that the optimal scale for the type of spruce trees in plot S6 (heights from 12 to 22 m) is somewhere between 1:10000 and 1:15000. The images in 1:8000 had details that did not help in treetop positioning, but may be needed for example in species recognition with texture measures.

Parameter f_{HDOM} corrects the local dominant height given by the CHM and thus defines the upper limit of search space. Similarly, the parameter *HDepth* defines the lower height and depth of the search space. Treetop positioning was tried at different values of these parameters. The optimal values for f_{HDOM} were from 1.1 to 1.3, when *HDepth* was kept at 0.65. All performance measures showed best performance in this range. Here, the CHM was calculated using a 5 m grid, which may be too coarse in sparse stands. Similarly, the density of the lidar data will most likely affect the quality of the CHM, which needs to be considered in setting the value for f_{HDOM}.

Parameter *HDepth* gives the lower height of the search space, and this parameter should be adjusted according to stand density since in dense stands only the tallest trees remain photo-visible The dominant height of plot S6 was 20.6 m and the shortest discernible tree had a plot-level relative height of 0.53. However, the neighboring trees of this 10.6-m high tree had heights from 15 to 18 m, which means that the local relative height of this tree is approximately 0.6. Best results in AI-% were obtained with *HDepth* at 0.65. Commission errors (“short ghost trees”) start to appear, if the search space is started from a too low height. If

Tab. 2: Performance of the 3D tree top positioning algorithm for different values of the parameter f_{HDOM}. Plot S6 with 95 trees in a circular plot with radius of 20 m. *Rlimit* = 1.41, *XYthin* = 1.5 and *HDepth* = 0.65. Four images in scale 1:12000.

f_{HDOM}	AI-%	c	Mean ΔZ, m	RMS ΔZ, m	RMS ΔXY, m	Trend ΔZ × h, m/m
0.95	46.3	21	+1.03	1.35	0.71	0.33
1.00	78.9	11	+0.88	1.28	0.69	0.31
1.05	88.4	7	+0.48	0.92	0.70	0.24
1.10	94.7	4	+0.21	0.74	0.69	0.18
1.15	93.7	5	+0.06	0.74	0.70	0.16
1.20	89.5	7	−0.09	0.80	0.70	0.17
1.25	90.5	5	−0.18	0.86	0.71	0.16
1.30	88.4	5	−0.21	0.85	0.71	0.14
1.35	85.3	6	−0.32	0.91	0.71	0.13
1.40	73.7	15	−0.39	0.93	0.72	0.13

Tab. 3: Performance of the 3D tree top positioning algorithm for different values of the parameter *HDepth*. Plot S6 with 95 trees in a circular plot with a radius of 20 m. *Rlimit* = 1.41, *XYthin* = 1.5 m, f_{HDOM} = 1.15. Four images in scale 1:12000.

HDepth	AI-%	c	Mean ΔZ, m	RMS ΔZ, m	RMS ΔXY, m	Trend ΔZ × h, m/m
0.45	64.2	31	+0.28	0.84	0.72	0.11
0.50	75.8	22	+0.19	0.77	0.71	0.11
0.55	88.4	10	+0.12	0.72	0.70	0.12
0.60	90.5	8	+0.06	0.71	0.70	0.13
0.65	93.7	5	+0.06	0.74	0.70	0.16
0.70	92.6	3	+0.01	0.75	0.70	0.19
0.75	89.5	3	−0.06	0.75	0.71	0.21
0.80	89.5	2	−0.21	0.77	0.72	0.22
0.85	82.1	3	−0.42	0.82	0.73	0.22
0.90	69.5	2	−0.70	0.94	0.74	0.20

the search space is not deep enough, the heights of the short trees are overestimated and the averaging effect increases. These effects are seen in Tab. 3.

4 Discussion

Semi-automatic 3D tree top positioning of individual trees using image-matching is an alternative or complement to lidar-based techniques in which trees are found by processing very high-resolution lidar data with from 5 to 30 points per m^2. The method presented here combines optical images and low-cost lidar with emphasis on the use of images. The lidar-based surface models that approximate the canopy elevation and give the terrain relief accurately are a necessity for accurate height estimation, since the ground is seldom seen in images taken under leaf-on conditions. If the image-matching strategy here is compared with common techniques of stereo matching for surface modelling, it can be said that the lidar CHM and DTM provided a short-cut and gave a good approximation for the possible space of solutions, which normally are obtained by hierarchical image matching techniques and the coarse-to-fine strategy (Schenk 1999). The results of the experiments gave support to the thesis that low-resolution lidar data can be used for delineating and bounding the search space in the canopy semi-automatically by adjusting the parameters that define the relative underestimation of the lidar-CHM (f_{HDOM}) and the lowest relative height of the trees that expected to be visible in the aerial views (*HDepth*).

The implementation described here is not very robust against the variation in the size of tree crowns and the results presented here were good mainly because the test stand represented a rather regular forest. In stands with a large species mixture and variation in crown sizes, the results have been found inferior. It may be possible to incorporate the use several sample trees (or synthetic images of crowns; see Larsen 1997) in image matching to improve the possibilities to detect and position trees of varying size. Similarly, it would be desirable, if the feature detector, template matching in this case, would yield not only the 2D image positions of tree tops but also symbolic information similar to what is utilized by an operator when the task is performed manually (species, crown size). It would then be possible to rule out automatically some of the unpreventable commission errors.

A semi-automatic approach seems to be the only solution to 3D tree top positioning using aerial views because of the nature of the problem. Occlusion and shading are inherently present in aerial views and trees vary in size, shape and radiometric properties. In the development of the methods presented here, the strategy has been to provide a system for measuring as many tree tops as possible automatically with a high positioning accuracy and a low commission error rate. After manual amendment the 3D tree tops provide tree heights and 2D image positions that can be used as seed points for the remaining tasks of species identification and measurement of crown dimensions, which can possibly be solved in the 2D image domain.

5 References

Baltsavias, E.P., 1999: A comparison between photogrammetry and laser scanning. – ISPRS, JPRS **54**(2-3): 83–94.

Culvenor, D.S., 2003: Extracting individual tree information: a survey of techniques for high spatial resolution imagery. – In: Wulder, M.A. & Franklin, S.E. (eds.): Remote Sensing of Forest Environments: Concepts and Case Studies. – pp. 255–277, KluwerAcademic, Boston.

Korpela, I., 2000: 3-d matching of tree tops using digitized panchromatic aerial photos. – Licentiate Thesis, 109 p., University of Helsinki, Department of Forest Resource Management.

Korpela, I., 2004: Individual tree measurements by means of digital aerial photogram-metry. – Silva Fennica Monographs **3**: 1–93.

Korpela, I., 2006: Geometrically accurate time series of archived aerial images and airborne lidar data in a forest environment. – Silva Fennica **40** (1): 109–126.

Korpela, I. & Tokola, T., 2006: Potential of aerial image-based monoscopic and multiview

single-tree forest inventory – a simulation approach. – Forest Science **52** (3): 136–147.

Larsen, M., 1997: Crown modeling to find tree top positions in aerial photographs. – In: Proceedings of the third International Airborne Remote Sensing Conference and Exhibition, Copenhagen, Denmark. – ERIM international **2**: 428–435.

Larsen, M. & Rudemo, M., 1998: Optimizing templates for finding trees in aerial photographs. – Pattern Recognition Letters **19** (12): 1153–1162.

Leckie, D.G., 1990: Advances in remote sensing technologies for forest surveys and management. – Canadian Journal of Forest Research **20** (4): 464–483.

Naesset, E., Gobakken, T., Holmgren, J., Hyyppä, H., Hyyppä, J., Maltamo, M., Nilsson, M., Olsson, H., Persson, Å. & Söderman, U., 2004: Laser scanning of forest resources: The Nordic experience. – Scandinavian Journal of Forest Research **19** (6): 482–499.

Pouliot, D.A., King, D.J., & Pitt, D.G., 2005: Development and evaluation of an automated tree detection-delineation algorithm for monitoring regenerating coniferous forests. – Canadian Journal of Forest Research **35** (10): 2332–2345.

Petrie, G., 2003: Airborne digital frame cameras. The technology is really improving. – GEOInformatics, 7(6), October/November 2003, pp.18–27.

Pollock, R.J., 1996: The automatic recognition of individual trees in aerial images of forests based on a synthetic tree crown model. – 158 p., PhD-thesis in computer science. The University of British Columbia.

Schenk, T., 1999: Digital photogrammetry. Vol I. – TerraScience, Laurelville, Ohio, USA.

St-Onge, B., Jumelet, J., Cobello, M. & Véga, C., 2004: Measuring individual tree height using acombination of stereophotogrammetry and lidar. – Canadian Journal of Forest Research **34**(10): 2122–2130.

Talts, J., 1977: Mätning i storskaliga flygbilder för beståndsdatainsamling. Summary: Photogrammetric measurements for stand cruising. – Royal College of Forestry, Department of Forest mensuration and management. Research notes NR 6 – 1977, 102 p. [Swedish]

Tarp-Johanssen, M.J., 2001: Locating Individual Trees in Even-aged Oak Stands by Digital Image processing of Aerial Photographs. – 158 p., PhD Thesis. Dept. of Mathematics and Physics, KVL, Copenhagen, Denmark.

Worley, D.P. & Landis, G.H., 1954: The accuracy of height measurements with parallax instruments on 1:12000 photographs. – Photogrammetric Engineering **20**(1): 823–829.

Address of the author:

Dr. Ilkka Korpela
Department of Forest Resource Management
POB 27, 00014 University of Helsinki, Finland –
e-mail: ilkka.korpela@helsinki.fi

Manuskript eingereicht: November 2006
Angenommen: November 2006